

EchoVLA: Robotic Vision-Language-Action Model with Synergistic Declarative Memory for Mobile Manipulation

Min Lin^{1*} Xiwen Liang^{1*} Bingqian Lin^{2*} Liu Jingzhi¹ Zijian Jiao¹ Kehan Li¹
 Yuhan Ma¹ Yuecheng Liu³ Shen Zhao¹ Yuzheng Zhuang³ Xiaodan Liang^{1†}

¹Shenzhen Campus of Sun Yat-sen University ²Shanghai Jiaotong University

³Huawei Noah’s Ark Lab

Abstract

Recent progress in Vision–Language–Action (VLA) models has enabled embodied agents to interpret multimodal instructions and perform complex tasks. However, existing VLAs are mostly confined to short-horizon, table-top manipulation, lacking the memory and reasoning capability required for long-horizon mobile manipulation, where agents must coordinate navigation and manipulation under changing spatial contexts. In this work, we present EchoVLA, a memory-aware VLA model for long-horizon mobile manipulation. EchoVLA incorporates a synergistic declarative memory inspired by the human brain, consisting of a scene memory that maintains a collection of spatial–semantic maps and an episodic memory that stores task-level experiences with multimodal contextual features. During both training and inference, the two memories are individually stored, updated, and retrieved based on current observations, task history, and instructions, and their retrieved representations are fused via coarse- and fine-grained attention to guide mobile–arm diffusion policies. To support large-scale training and evaluation, we further introduce MoMani, an automated benchmark that generates expert-level long-horizon trajectories through multi-modal large language model (MLLM)–guided planning and feedback-driven refinement, supplemented with real-robot demonstrations. Experiments in simulated and real-world settings show that EchoVLA improves long-horizon performance, reaching 0.52 SR on manipulation/navigation and 0.31 on mobile manipulation, exceeding $\pi_{0.5}$ by +0.08 and +0.11.

1. Introduction

Recent advances in Vision–Language–Action (VLA) models [3, 5, 12, 18, 20, 34, 36, 39, 47] have shown strong

potential for general-purpose robot learning, enabling embodied agents to interpret multimodal inputs and perform diverse manipulation tasks. Models such as RT-2 [48], OpenVLA [22], and ManipLLM [26] demonstrate that large-scale vision–language pretraining can be extended to robot control, achieving impressive zero-shot generalization across unseen objects and scenes. However, most existing VLAs are restricted to short-horizon, table-top manipulation, and rely on Markovian control, where each decision depends solely on the current observation. This limitation prevents consistent reasoning over extended task sequences and hinders long-term spatial understanding.

To overcome this limitation, we draw inspiration from the declarative memory system in the human brain, which comprises complementary subsystems for spatial and experiential encoding. The parahippocampal cortex (PHC) and related retrosplenial regions represent the spatial and semantic structure of scenes, providing contextual information about environmental layouts and object relations [2, 14, 15]. These regions project to the hippocampus, which integrates contextual inputs into temporally organized episodic traces that capture individual experiences and task outcomes [13, 33]. Such a dual-system interaction allows humans to remember where things are and how tasks were accomplished—offering a useful analogy for memory-guided embodied reasoning.

Building on this insight, we propose EchoVLA, a memory-aware Vision–Language–Action model for long-horizon mobile manipulation. EchoVLA introduces two complementary memory modules: a **scene memory** parallels the PHC by maintaining a collection of spatial–semantic maps across different scenes, and an **episodic memory** mirrors hippocampal processing by storing task-level experiences with multimodal contextual features. As shown in Figure 1, this design contrasts with prior decoder- and diffusion-based approaches by explicitly integrating memory-guided attention into the control pipeline. During both training and inference, the two memories are independently stored, updated, and retrieved based on current ob-

*Equal contribution.

†Corresponding author.

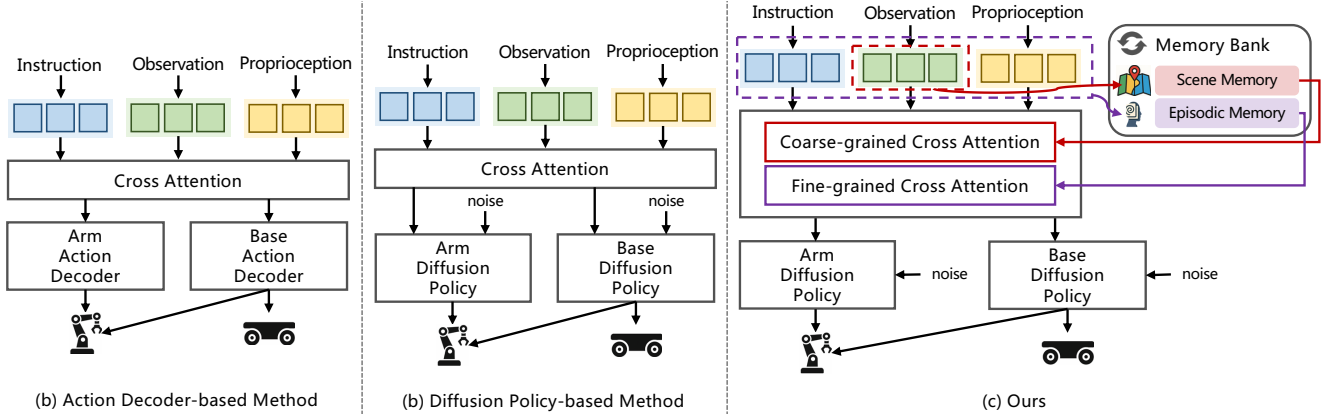


Figure 1. Comparison of mobile manipulation control paradigms. (a) Action-decoder methods [22, 48] use a single cross-attention module to regress arm and base actions. (b) Diffusion-policy methods [10, 44] replace action decoders with denoisers but rely only on current observations. (c) EchoVLA (ours) augments diffusion policies with dual memories, using coarse attention over scene memory and fine attention over episodic memory to provide context-aware action generation.

servations, task history, and language instructions. Their retrieved representations are then fused through coarse- and fine-grained attention to guide the mobile-arm diffusion policies. Through this neuro-inspired declarative memory design, EchoVLA maintains both spatial continuity and temporal reasoning, enabling non-Markov decision-making and generalization across long-horizon mobile manipulation tasks.

We further introduce MoMani, an automated benchmark for mobile manipulation that generates expert-level long-horizon trajectories via MLLM-guided planning and feedback-based refinement. Compared with existing mobile manipulation benchmarks—which remain limited in scale and task diversity—as well as datasets like RoboTwin 2.0 [9] and RoboCasa [30], MoMani offers richer task coverage and collects real-robot demonstrations on a holonomic mobile platform [43], providing a realistic and scalable testbed for embodied reasoning and control.

Our contributions are summarized as follows:

- We propose EchoVLA, a memory-aware VLA model equipped with synergistic scene and episodic memory for long-horizon mobile manipulation.
- We introduce MoMani, an automated benchmark that provides expert-level multimodal trajectories and real-robot demonstrations for scalable embodied data generation and evaluation.
- We conduct extensive simulated and real-world experiments, showing that EchoVLA consistently outperforms strong baselines on long-horizon tasks.

2. Related Work

2.1. Mobile Manipulation Benchmark

Early embodied benchmarks such as RoboTHOR [11] for sim-to-real indoor navigation and iGibson 2.0 [23] for object-centric household tasks mainly offer mobile percep-

tion and basic interaction. Habitat 2.0 [38] further supports interactive rearrangement with articulated objects, but the mobile-manipulation coupling is still limited to pre-defined skills. Large-scale suites like BEHAVIOR-100 / 1K [24, 37] and ManiSkill2 [16] broaden the task families to 100–1000 household activities or 20+ manipulation families, yet most tasks assume a fixed or simplified manipulation setting rather than full mobile manipulation. More recent, robotics-oriented simulators move closer to real mobile manipulation: RoboCasa [30] targets realistic kitchen scenes with 120+ layouts and 2,500+ assets but the task spectrum is still mostly kitchen rearrangement; MoMa-Kitchen [46] provides 100K+ affordance-grounded samples for “last-mile” base positioning but is domain-specific to kitchens; RoboTwin 2.0 [9] automates data generation for 50 dual-arm tasks in 731-object settings but does not involve base navigation; TidyBot [42] shows LLM-guided, user-conditioned tidy-up on a mobile manipulator, while TidyBot++ [43] mainly contributes an open-source holonomic mobile-manipulation platform for data collection rather than a broad, automatic task generator. Compared with these, MoMani provides a unified, automated pipeline that produces expert-level trajectories for diverse mobile-manipulation tasks and augments them with real-robot demonstrations.

2.2. Vision-Language-Action Model

Driven by advances in visual–language foundation models [7, 28, 32] and large-scale robot datasets [6, 31], Vision–Language–Action (VLA) models unify perception, reasoning, and control within a single multimodal policy. Representative works such as RT-2 [48], OpenVLA [22], and ManipLLM [26] discretize continuous actions into token sequences and perform autoregressive prediction, enabling large-scale pretraining but limiting motion continuity. Recent approaches (e.g., CogACT [25], DexVLA

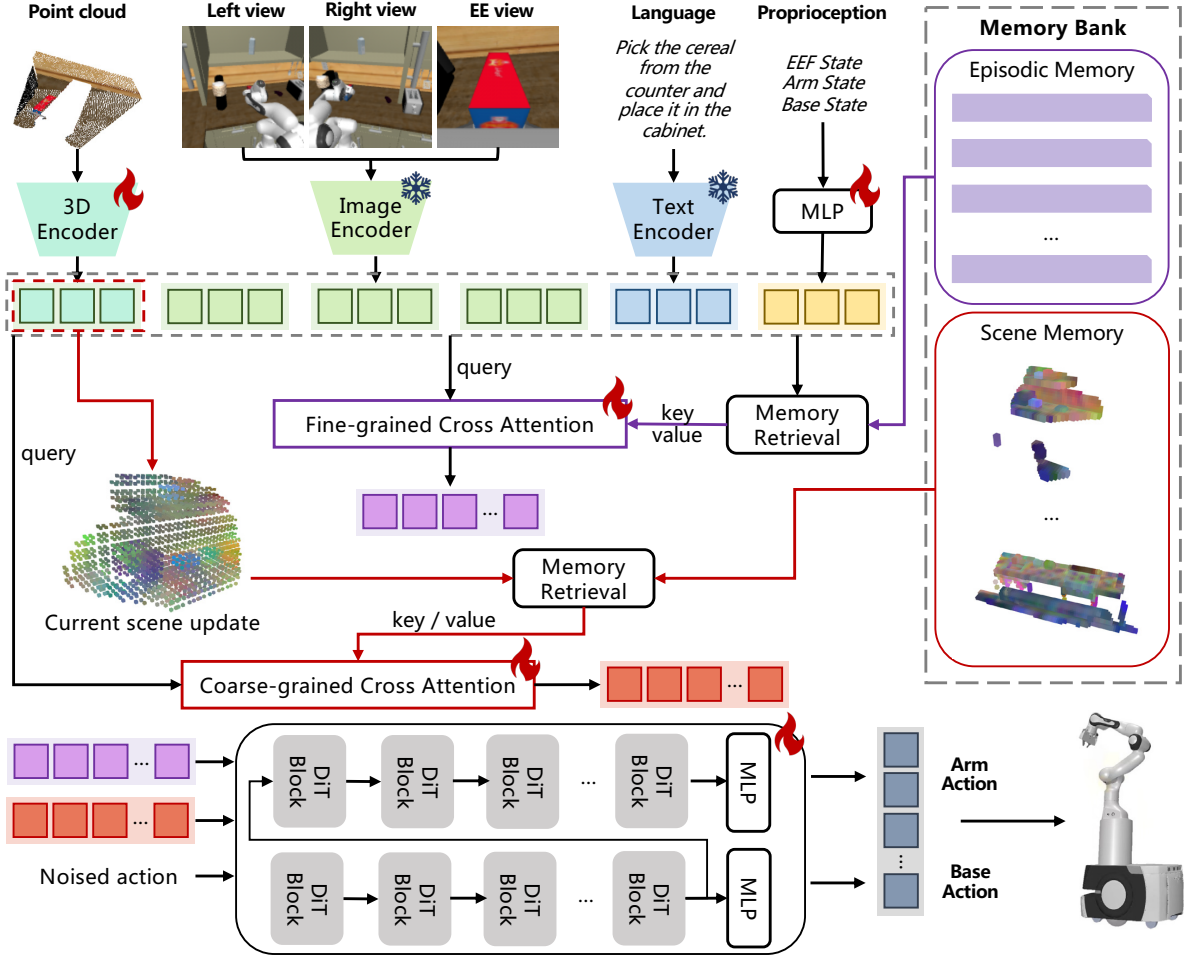


Figure 2. Overview of EchoVLA. Multi-modal observations (RGB views, point clouds, language, and proprioception) are encoded into a unified token sequence. The model retrieves relevant information from both episodic and scene memory through coarse- and fine-grained cross-attention. The retrieved memory augments the diffusion policy, which generates base and arm actions through a per-part denoising process.

[41], HybridVLA [27]) introduce diffusion- or regression-based action heads to capture the multimodal distribution of robot trajectories, while AC-DiT [8] explicitly models coordination between the mobile base and the manipulator through adaptive diffusion. Notable works π_0 and $\pi_{0.5}$ [4, 19] address hierarchical trajectory diffusion for mobile manipulation. π_0 models the full robot action space, while $\pi_{0.5}$ introduces per-part decomposition for mobile base and manipulator, adding partial episodic memory. Despite improved trajectory fidelity, both lack explicit scene-level memory for long-horizon planning. Meanwhile, AnywhereVLA [17] adopts a modular design that combines classical SLAM with a fine-tuned VLA head for robust real-world pick-and-place, highlighting the practicality of hybrid systems. However, most existing VLAs remain Markovian, relying only on current observations without structured memory for long-horizon reasoning.

To address this, MemoryVLA [35] augments VLAs with a perceptual–cognitive memory that caches visual features

to enhance manipulation stability. However, its memory remains an implicit perceptual cache without an explicit spatial representation or task-level experience storage, limiting its ability to reason over long-horizon tasks. In contrast, EchoVLA introduces a synergistic declarative memory composed of scene and episodic components. The scene memory explicitly constructs a spatial–semantic map of object layouts and environmental structure, while the episodic memory records task-specific experience traces for contextual retrieval. This dual-memory mechanism enables long-horizon reasoning in mobile-manipulation tasks beyond the capability of prior single-memory VLAs.

3. EchoVLA

EchoVLA is a memory-augmented vision–language–action framework designed for long-horizon mobile manipulation. Its key idea is to maintain two complementary memory systems—scene memory and episodic memory—and integrate them into a coarse-to-fine retrieval hierarchy that improves

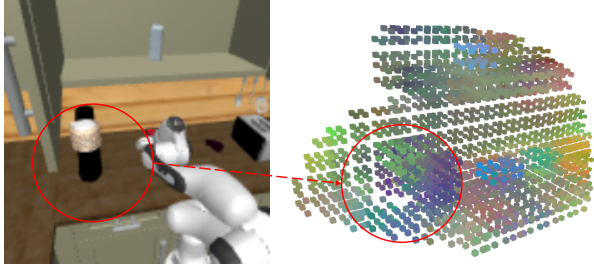


Figure 3. Visualization of the voxelized 3D feature map, which encodes local geometric structure from depth observations.

spatial consistency, temporal reasoning, and manipulation precision. The overall architecture as illustrated in Figure 2 consists of: (1) multimodal state representation, (2) memory retrieval and interaction, and (3) diffusion-based action generation. We describe each component in detail.

3.1. Problem Formulation

At timestep t , the agent observes multi-view RGB-D images \mathcal{O}_t , proprioceptive states \mathbf{s}_t , and a natural-language instruction \mathcal{I} . The goal is to output continuous arm and base actions:

$$(a_t^{\text{arm}}, a_t^{\text{base}}) = \pi_\theta(\mathcal{I}, \mathcal{O}_{1:t}, \mathbf{s}_{1:t}). \quad (1)$$

Long-horizon tasks are non-Markovian—two visually similar frames may correspond to completely different progress states (e.g., “cabinet opened” vs. “about to open”). Thus, a memory mechanism is needed.

3.2. Multimodal State Representation

EchoVLA encodes language, appearance, 3D structure, and robot configuration into a unified token sequence that drives memory retrieval and action generation. Each modality is processed with a dedicated backbone: language and multi-view RGB images use frozen SigLIP encoders [45], while 3D structure is modeled by a task-adaptive PointAttn network [40].

The instruction is encoded using the text tower of SigLIP, producing language tokens \mathbf{L} without updating the pre-trained parameters. Multi-view RGB images from three fixed cameras are processed independently by the SigLIP vision tower, also kept frozen, yielding per-view features $\mathbf{V}_t^{(i)}$. These tokens preserve SigLIP’s cross-modal alignment, allowing the policy and memory modules to reason within a consistent semantic embedding space. The view-specific tokens are concatenated and projected into a shared feature space to form \mathbf{V}_t .

Depth observations are fused into a point cloud, which is encoded by a trainable PointAttn backbone. [40]. The resulting tokens \mathbf{P}_t provide fine-grained geometric cues—such as free-space structure, support surfaces, and object boundaries—and adapt to the specific robot embodiment and scene characteristics, complementing the frozen SigLIP features with manipulable 3D information.

The proprioceptive state \mathbf{s}_t is transformed into tokens \mathbf{R}_t using a small MLP, supplying the model with the robot’s internal configuration. We then form a unified token sequence:

$$\mathbf{S}_t = [\mathbf{L}, \mathbf{V}_t, \mathbf{P}_t, \mathbf{R}_t], \quad (2)$$

which serves as the query for hierarchical memory retrieval and conditions the diffusion policy.

3.3. Memory Retrieval and Interaction

EchoVLA maintains two complementary memory banks—scene memory and episodic memory—and retrieves information from them using a two-level hierarchical (coarse-to-fine) attention mechanism. The hierarchy comes from the semantic granularity of the two memories: scene memory provides slowly varying spatial structure, while episodic memory captures fine-grained, time-indexed task progress. The retrieved memory features are later fused with the current tokens and used to condition the diffusion policy.

3.3.1. Scene Memory

Scene memory maintains a voxelized 3D feature map that accumulates spatial information across episodes within the same environment. Instead of storing features in temporal order, the memory represents a persistent, environment-specific 3D structure that is refined as new episodes unfold. At the beginning of training in a new environment, the memory is initialized as an empty voxel grid. As the agent interacts with the environment across multiple episodes, depth observations are aggregated into this voxel grid and encoded by the PointAttn network, producing a 3D feature volume (see Figure 3):

$$\mathbf{V}_t^{3D} \in \mathbb{R}^{X \times Y \times Z \times C}. \quad (3)$$

To incorporate new observations while avoiding redundant updates, the memory applies a discrepancy-driven rule: the current voxel features \mathbf{V}_t^{3D} are compared with a reconstruction generated from the existing memory. Regions whose reconstruction error exceeds a threshold are updated with the new PointAttn features, while unchanged areas retain their previous values. This update mechanism allows the scene map to evolve consistently across episodes, gradually converging to a stable representation of the environment’s geometry.

During inference, the scene memory continues to refine itself using the same discrepancy-based rule, enabling the model to adapt online if the environment differs from the training episodes or undergoes rearrangement. The resulting memory provides a compact but spatially coherent representation of the scene, capturing structural elements such as surfaces, free space, and container geometry that remain stable across episodes but are not fully observable in any single timestep.

3.3.2. Episodic Memory

Episodic memory stores a short horizon of recent token sequences, each associated with its timestep. Formally, we maintain a time-indexed buffer:

$$\mathcal{M}^{\text{epi}} = \{(\mathbf{S}_{t-k}, t-k), \dots, (\mathbf{S}_{t-1}, t-1)\}, \quad (4)$$

where the window size k is determined by the memory capacity.

Unlike scene memory, which evolves slowly and captures stable 3D structure, episodic memory preserves fine-grained temporal information tied to recent interactions—such as whether a drawer has been opened, whether an object has already been grasped, or the precise end-effector configuration in the immediate past. The memory is maintained as a fixed-size FIFO buffer updated at each timestep, ensuring that temporally coherent information is retained while avoiding unbounded growth. By storing the original encoded tokens instead of compressing them into abstract summaries, the model preserves detailed temporal cues that are essential for resolving non-Markov ambiguities and maintaining consistent task execution across visually similar states.

3.3.3. Memory Matching and Attention

EchoVLA accesses its two memory banks in two steps: it first matches the current representations to memory entries using cosine similarity, and then interacts with the selected entries via cross-attention.

For scene memory, the query is the current voxelized 3D feature map \mathbf{V}_t^{3D} . We compute cosine similarity between \mathbf{V}_t^{3D} and stored scene maps in $\mathcal{M}^{\text{scene}}$, select the top- k matches $\mathcal{M}_{\text{sel}}^{\text{scene}}$, and apply coarse cross-attention:

$$\mathbf{Z}_t^{\text{scene}} = \text{CrossAttn}(\mathbf{q} = \mathbf{V}_t^{3D}, \mathbf{k} / \mathbf{v} = \mathcal{M}_{\text{sel}}^{\text{scene}}). \quad (5)$$

For episodic memory, the query is the current multimodal state tokens \mathbf{S}_t . We match \mathbf{S}_t to historical states in \mathcal{M}^{epi} , select the most relevant subset $\mathcal{M}_{\text{sel}}^{\text{epi}}$, and apply fine cross-attention:

$$\mathbf{Z}_t^{\text{epi}} = \text{CrossAttn}(\mathbf{q} = \mathbf{S}_t, \mathbf{k} / \mathbf{v} = \mathcal{M}_{\text{sel}}^{\text{epi}}). \quad (6)$$

The outputs of the two interactions are combined into a memory-augmented representation:

$$\mathbf{H}_t = [\mathbf{Z}_t^{\text{scene}}, \mathbf{Z}_t^{\text{epi}}], \quad (7)$$

which serves as the conditioning input for the diffusion-based action policy.

3.4. Diffusion-based Action Generation

To model the heterogeneous dynamics of mobile-base motion and arm manipulation, we propose a per-part diffusion policy conditioned on the memory-augmented representation \mathbf{H}_t .

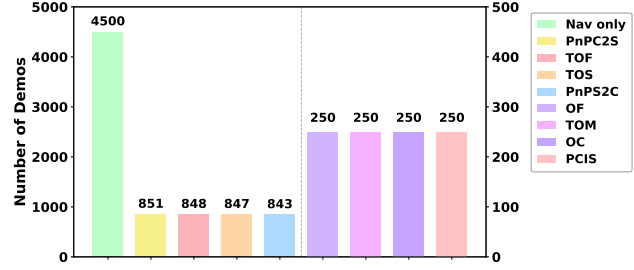


Figure 4. Dataset composition across simulation and real-world tasks. The simulation set includes four mobile manipulation tasks (TOF, PnPS2C, PnPC2S, TOS) and a large pure-navigation subset. The real-world tasks (OF, TOM, OC, PCIS) involve mobile manipulation.

Each action subspace $p \in \{\text{base, arm}\}$ is generated by an independent denoising diffusion process. For part p , the denoiser predicts the noise of a perturbed action sample:

$$\epsilon_{\theta}^{(p)} = \text{Denoiser}_p(\mathbf{z}_t, \mathbf{H}_t, t), \quad p \in \{\text{base, arm}\} \quad (8)$$

where \mathbf{z}_t is the noisy action at diffusion step t , \mathbf{H}_t captures the fused current observation with retrieved scene-level and episodic context.

During training, the objective minimizes the denoising loss for each part:

$$\mathcal{L} = \sum_{p \in \{\text{base, arm}\}} \mathbb{E}_{t, \mathbf{z}_t} \left[\|\epsilon - \epsilon_{\theta}^{(p)}(\mathbf{z}_t, \mathbf{H}_t, t)\|^2 \right]. \quad (9)$$

This per-part design enables structured action generation, allowing coordinated yet decoupled learning of locomotion and manipulation behaviors, which improves scene generalization and cross-task transfer.

4. MoMani

We introduce MoMani, an automated mobile manipulation benchmark that enables efficient and high-quality data generation for embodied agents. Compared with existing datasets such as RoboTwin 2.0 [9], which mainly focus on static manipulation, and RoboCasa [30], which include a limited range of task types, MoMani provides a unified pipeline that automatically produces expert-level trajectories across diverse mobile manipulation tasks. The benchmark combines MLLM[1]-guided planning with feedback-driven refinement to generate coherent long-horizon trajectories without human intervention. In addition to simulated data, we also collect a set of real-robot demonstrations to enhance the realism and applicability of the benchmark.

4.1. Simulation Data Construction

The simulation dataset of MoMani is generated through an automated pipeline that synthesizes expert-level trajectories under diverse environment configurations. The process begins with a task program generation module, where

a MLLM receives natural-language instructions and available object information, and then outputs executable task scripts composed of atomic manipulation and navigation primitives. These scripts are executed in a physics simulator, and the resulting state changes are continuously monitored to ensure successful completion of each sub-goal.

When a failure occurs, such as an invalid grasp pose or an unsatisfied task condition, the system collects the execution log and visual feedback, analyzes the failure cause, and revises the corresponding code segment. This closed-loop refinement continues until all goals are achieved or a retry limit is reached, producing verified trajectories with minimal human intervention. Each successful trajectory is stored together with synchronized RGB-D observations, object states, and robot joint data to form multimodal training samples.

To enrich scene diversity and improve policy robustness, MoMani performs domain randomization along multiple dimensions, including object layout, surface texture, lighting, and clutter density. All physical parameters are randomized within feasible bounds to ensure stability while maintaining task realism.

4.2. Real-Robot Demonstration Collection

To bridge the gap between simulation and the physical world, we further collect a real-robot dataset following the hardware configuration and control framework introduced in TidyBot++ [43]. Our platform consists of a Kinova Gen3 7-DoF manipulator mounted on a holonomic mobile base, allowing omnidirectional movement and stable arm-base coordination. The system is equipped with a front-mounted RGB-D camera for local perception and a top-view stereo pair for scene understanding and visual tracking. All sensors are time-synchronized through a unified ROS-based logging system, ensuring accurate correspondence between visual and proprioceptive data streams.

We employ a web-based teleoperation interface that allows intuitive control of both the arm and the base. Operators perform high-level manipulation behaviors such as object relocation, container organization, and surface clearing by guiding the robot through natural motions. During teleoperation, the system records RGB-D images, base odometry, joint angles, gripper states, and end-effector poses at 30 Hz. Each trajectory is automatically segmented into motion primitives (approach, grasp, lift, place) using velocity and contact cues. Failed attempts or unstable grasps are discarded, while successful executions are verified through replay.

We further summarize the distribution of demonstrations in Figure 4. Our simulation dataset contains four mobile manipulation tasks (PnPCounterToStove, PnPSinkToCounter, TurnOnFaucet, TurnOnStove) together with a large navigation-only subset. The real-world portion in-

cludes four mobile manipulation tasks corresponding to OpenFridge, TurnOnMicrowave, OpenDrawer, and PutCu-pIntoSink.

5. Experiment

5.1. Experimental Setup

We evaluate our proposed EchoVLA model in both simulation and real-world environments. In simulation, experiments are conducted in the RoboCasa simulator using multiple mobile manipulation tasks.

For real-world experiments, we set up a 7m \times 7m test arena containing a variety of household-like task scenarios. The real robot platform is built upon the open-source *TidyBot++* mobile manipulator, on which we deploy EchoVLA to execute the tasks.

In terms of training, EchoVLA is trained on 8 NVIDIA A100 GPUs with observations including multi-view RGB-D images and robot states, while the action space is decomposed into mobile base and arm actions following the per-part diffusion design.

5.2. Comparison with Baselines in RoboCasa Simulation

We evaluate EchoVLA against several representative baselines for mobile manipulation in the RoboCasa simulator. These baselines cover a diverse range of imitation and diffusion-based policy architectures: **BC-T** [29], **Diffusion Policy** [10], **DP3** [44], $\pi_{0.5}$ [19], and **WB-VIMA** [21].

We evaluate EchoVLA on representative RoboCasa tasks including **PnPCounterToStove**, **PnPSinkToCounter**, **TurnOnFaucet**, and **TurnOnStove**, which involve similar manipulation skills across partially overlapping kitchen scenes. For navigation, we use the standard **NavigateKitchen** task. For the **Mobile Manipulation** setting, we further increase difficulty by initializing the robot far from target objects or adding a follow-up navigation step after completing the initial manipulation (e.g., turn on a stove, then move to another location).

We compare performance across three task categories: (1) **Manipulation**, focusing on arm-only actions; (2) **Navigation**, emphasizing base motion precision; and (3) **Mobile Manipulation**, involving coordinated base-arm control. Across all three categories, we report the **Success Rate (SR)** as the unified evaluation metric. All results are averaged over three random seeds and **50 evaluation episodes** for statistical robustness.

Specifically, all results for both **Manipulation and Navigation** tasks and **Mobile Manipulation** tasks are now unified and summarized in Table 1. This consolidated presentation highlights the performance differences across task categories and emphasizes the increased difficulty inherent in mobile manipulation tasks. The results in Table 1 reveal

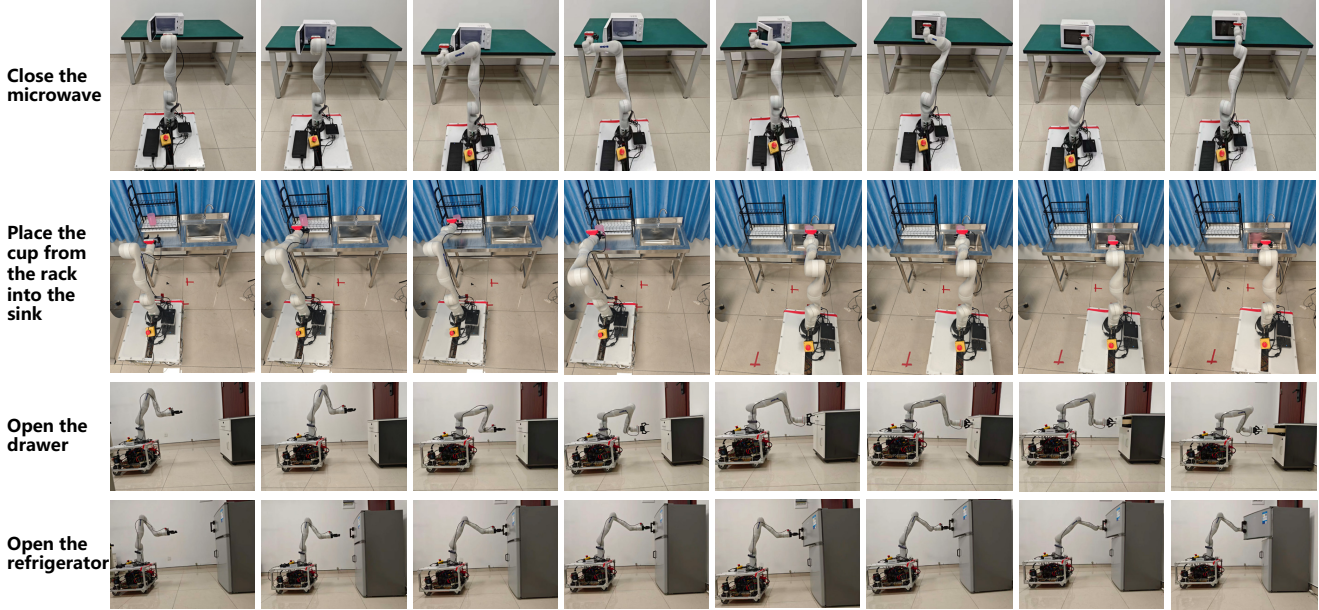


Figure 5. Real-world rollouts generated by EchoVLA. The robot successfully completes four mobile manipulation tasks—turning off the microwave, placing the cup from the rack into the sink, opening the drawer, and opening the refrigerator.

Table 1. Success Rate (SR) across two task families: (1) Manipulation/Navigation tasks and (2) Mobile Manipulation tasks. Results are averaged over 50 episodes. The row highlighted in light green indicates our proposed method.

Method	PnPC2S	PnPS2C	TOF	TOS	Nav only	Avg	
Manipulation / Navigation	BC-T	0.04	0.46	0.33	0.45	0.10	0.28
	Diffusion Policy	0.00	0.00	0.03	0.00	0.03	0.01
	DP3	0.03	0.25	0.43	0.26	0.13	0.22
	WB-VIMA	0.00	0.12	0.11	0.19	0.31	0.15
	$\pi_{0.5}$	0.13	0.62	0.45	0.68	0.31	0.44
Mobile Manipulation	EchoVLA (Ours)	0.21	0.68	0.51	0.67	0.51	0.52
	BC-T	0.00	0.11	0.04	0.04	-	0.05
	DP3	0.00	0.10	0.08	0.04	-	0.06
	WB-VIMA	0.00	0.12	0.11	0.19	-	0.11
	$\pi_{0.5}$	0.08	0.25	0.18	0.27	-	0.20
	EchoVLA (Ours)	0.17	0.34	0.29	0.43	-	0.31

several important observations:

1) Method Comparison. For Manipulation and Navigation tasks, traditional behavior cloning (BC-T) and Diffusion Policy exhibit low performance, with Diffusion Policy often achieving near-zero success rates. $\pi_{0.5}$ shows improved performance, while our proposed EchoVLA achieves the highest average success rate (Avg Success = 0.52), demonstrating robust task execution.

2) Increased Difficulty in Mobile Manipulation. Compared to Manipulation and Navigation tasks, success rates in Mobile Manipulation tasks drop noticeably. For example, $\pi_{0.5}$'s Avg Success decreases from 0.47 to 0.36, and BC-T achieves almost no successful outcomes. This indicates that coordinating base and arm control significantly increases task complexity.

3) Advantage of EchoVLA. Despite the increased diffi-

Table 2. Ablation results over different observation modalities and memory modules, including RGB, Point Cloud (PC), Episodic Memory (EM), and Scene Memory (SM). Performance is evaluated on two representative tasks: **PnP Counter To Stove (Mobile)** and **PnP Counter To Stove**. All numbers indicate **Success Rate (SR)**, averaged over 50 episodes.

Observation / Memory				Task	
RGB	PC	EM	SM	PnPC2S (Mobile)	PnPC2S
✗	✓	✓	✓	0.02	0.13
✓	✗	✓	✓	0.08	0.15
✓	✓	✓	✗	0.09	0.16
✓	✓	✗	✓	0.14	0.13
✓	✓	✓	✓	0.17	0.21

Table 3. Success rates for real robot mobile manipulation tasks across four actions. (Note: OD = Open Drawer, CM = Close Microwave, TC = Take Cup to Sink, OR = Open Refrigerator Door. Avg SR = average success rate across available actions.)

Method	OD	CM	TC	OR	Avg SR
$\pi_{0.5}$	0.35	0.55	0.20	0.50	0.40
Diffusion	0.40	0.60	0.50	0.30	0.45
Ours	0.45	0.70	0.50	0.40	0.51

culty, EchoVLA maintains the highest success rate (0.45) in Mobile Manipulation tasks, outperforming all other methods. This highlights the method’s effectiveness in handling coordinated base-arm motion, long-range navigation, and sequential manipulation tasks.

4) Task-specific Performance Variations. Tasks such as PnP Sink To Counter and TurnOn Faucet show larger performance variations across methods, reflecting higher requirements for spatial understanding and precise manipulation. EchoVLA consistently achieves strong performance on these challenging tasks, demonstrating its capability in multi-modal perception and action reasoning.

5.3. Ablation Study

Ablations are performed on two representative RoboCasa tasks, **PnP Counter to Stove (Mobile)** and **PnP Counter to Stove**, and results are reported as **Success Rate (SR)** averaged over 50 episodes.

1) Observation Ablation. We examine the effect of removing point cloud input from the observation space. When the agent relies solely on RGB features without 3D geometric cues, its spatial grounding ability decreases notably. As shown in Table 2, removing point cloud input results in

consistent performance drops across both mobile and non-mobile variants, demonstrating the importance of geometric depth information for accurate object localization and grasping.

2) Memory Module Ablation. We further analyze the roles of our two memory mechanisms: **Episodic Memory (EM)** and **Scene Memory (SM)**. The ablation rows in Table 2 show that disabling either EM or SM leads to substantial degradation, and removing both RGB or PC signals further compounds these effects. Overall, the results highlight that observation diversity (RGB + PC) and hierarchical memory (EM + SM) are both essential for robust performance in manipulation and mobile manipulation tasks in RoboCasa.

5.4. Real Robot Experiment

Task Complexity Analysis. Although OR (189.53 frames) and OD (190.98 frames) have similar trajectory lengths, OR is substantially more complex. It requires precise handle grasping, state transitions, side navigation with collision avoidance, and sustained force to open the door. OD mainly involves coordinated base motion and a single pulling action. This distinction explains why $\pi_{0.5}$ performs better on multi-step tasks like OR, whereas Diffusion Policy is more effective for smoother, continuous manipulations.

Real-World Performance. Table 3 reports success rates on four real-robot mobile manipulation tasks. EchoVLA achieves the highest average success rate (0.51), outperforming both $\pi_{0.5}$ (0.40) and Diffusion Policy (0.45) across most tasks. In particular, EchoVLA exhibits strong performance on Close Microwave (0.70) and Take Cup (0.50), demonstrating effective integration of memory-guided perception and control. EchoVLA also shows reliable execution in real-world deployments, as illustrated by the rollouts in Figure 5.

6. Conclusion

We presented EchoVLA, a memory-aware vision–language–action framework for long-horizon mobile manipulation. EchoVLA combines a scene memory that preserves 3D spatial structure with an episodic memory that captures recent task context, enabling a memory-augmented diffusion policy to handle non-Markov decision-making and generalize across diverse tasks. We also introduce MoMani, a new benchmark covering both procedurally generated simulation tasks and real-robot evaluations. Extensive experiments demonstrate consistent improvements over strong baselines.

Limitations EchoVLA depends on depth observations to build its scene memory, and may be sensitive to noisy or incomplete depth inputs, which could lead to degraded performance in cluttered or low-visibility environments.

References

- [1] Josh Achiam, Steven Adler, Sandhini Agarwal, Lama Ahmad, Ilge Akkaya, Florencia Leoni Aleman, Diogo Almeida, Janko Altenschmidt, Sam Altman, Shyamal Anadkat, et al. Gpt-4 technical report. *arXiv preprint arXiv:2303.08774*, 2023. 5
- [2] Elissa M Aminoff, Kestutis Kveraga, and Moshe Bar. The role of the parahippocampal cortex in cognition. *Trends in cognitive sciences*, 17(8):379–390, 2013. 1
- [3] Johan Bjorck, Fernando Castañeda, Nikita Cherniadev, Xingye Da, Runyu Ding, Linxi Fan, Yu Fang, Dieter Fox, Fengyuan Hu, Spencer Huang, et al. Gr0ot n1: An open foundation model for generalist humanoid robots. *arXiv preprint arXiv:2503.14734*, 2025. 1
- [4] Kevin Black, Noah Brown, Danny Driess, Adnan Esmail, Michael Equi, Chelsea Finn, Niccolò Fusai, Lachy Groom, Karol Hausman, Brian Ichter, Szymon Jakubczak, Tim Jones, Liyiming Ke, Sergey Levine, Adrian Li-Bell, Mohith Mothukuri, Suraj Nair, Karl Pertsch, Lucy Xiaoyang Shi, James Tanner, Quan Vuong, Anna Walling, Haohuan Wang, and Ury Zhilinsky. π_0 : A vision-language-action flow model for general robot control, 2024. 3
- [5] Anthony Brohan, Noah Brown, Justice Carbajal, Yevgen Chebotar, Joseph Dabis, Chelsea Finn, Keerthana Gopalakrishnan, Karol Hausman, Alex Herzog, Jasmine Hsu, et al. Rt-1: Robotics transformer for real-world control at scale. *arXiv preprint arXiv:2212.06817*, 2022. 1
- [6] Qingwen Bu, Jisong Cai, Li Chen, Xiuqi Cui, Yan Ding, Siyuan Feng, Shenyuan Gao, Xindong He, Xuan Hu, Xu Huang, et al. Agibot world colosseo: A large-scale manipulation platform for scalable and intelligent embodied systems. *arXiv preprint arXiv:2503.06669*, 2025. 2
- [7] Mathilde Caron, Hugo Touvron, Ishan Misra, Hervé Jégou, Julien Mairal, Piotr Bojanowski, and Armand Joulin. Emerging properties in self-supervised vision transformers. In *Proceedings of the IEEE/CVF international conference on computer vision*, pages 9650–9660, 2021. 2
- [8] Sixiang Chen, Jiaming Liu, Siyuan Qian, Han Jiang, Lily Li, Renrui Zhang, Zhuoyang Liu, Chenyang Gu, Chengkai Hou, Pengwei Wang, et al. Ac-dit: Adaptive coordination diffusion transformer for mobile manipulation. *arXiv preprint arXiv:2507.01961*, 2025. 3
- [9] Tianxing Chen, Zanxin Chen, Baijun Chen, Zijian Cai, Yibin Liu, Zixuan Li, Qiwei Liang, Xianliang Lin, Yiheng Ge, Zhenyu Gu, et al. Robotwin 2.0: A scalable data generator and benchmark with strong domain randomization for robust bimanual robotic manipulation. *arXiv preprint arXiv:2506.18088*, 2025. 2, 5
- [10] Cheng Chi, Zhenjia Xu, Siyuan Feng, Eric Cousineau, Yilun Du, Benjamin Burchfiel, Russ Tedrake, and Shuran Song. Diffusion policy: Visuomotor policy learning via action diffusion, 2024. 2, 6, 3
- [11] Matt Deitke, Winson Han, Alvaro Herrasti, Aniruddha Kembhavi, Eric Kolve, Roozbeh Mottaghi, Jordi Salvador, Dustin Schwenk, Eli VanderBilt, Matthew Wallingford, et al. Robothor: An open simulation-to-real embodied ai platform. In *Proceedings of the IEEE/CVF conference on computer vision and pattern recognition*, pages 3164–3174, 2020. 2
- [12] Pengxiang Ding, Jianfei Ma, Xinyang Tong, Binghong Zou, Xinxin Luo, Yiguo Fan, Ting Wang, Hongchao Lu, Panzhong Mo, Jinjin Liu, et al. Humanoid-vla: Towards universal humanoid control with visual integration. *arXiv preprint arXiv:2502.14795*, 2025. 1
- [13] Howard Eichenbaum. On the integration of space, time, and memory. *Neuron*, 95(5):1007–1018, 2017. 1
- [14] Russell Epstein and Nancy Kanwisher. A cortical representation of the local visual environment. *Nature*, 392(6676):598–601, 1998. 1
- [15] Russell A Epstein. Parahippocampal and retrosplenial contributions to human spatial navigation. *Trends in cognitive sciences*, 12(10):388–396, 2008. 1
- [16] Jiayuan Gu, Fanbo Xiang, Xuanlin Li, Zhan Ling, Xiqiang Liu, Tongzhou Mu, Yihe Tang, Stone Tao, Xinyue Wei, Yunchao Yao, et al. Maniskill2: A unified benchmark for generalizable manipulation skills. *arXiv preprint arXiv:2302.04659*, 2023. 2
- [17] Konstantin Gubernatorov, Artem Voronov, Roman Voronov, Sergei Pasynkov, Stepan Perminov, Ziang Guo, and Dzmitry Tsetserukou. Anywherevla: Language-conditioned exploration and mobile manipulation, 2025. 3
- [18] Wenlong Huang, Chen Wang, Ruohan Zhang, Yunzhu Li, Jiajun Wu, and Li Fei-Fei. Voxposer: Composable 3d value maps for robotic manipulation with language models. *arXiv preprint arXiv:2307.05973*, 2023. 1
- [19] Physical Intelligence, Kevin Black, Noah Brown, James Darpinian, Karan Dhabalia, Danny Driess, Adnan Esmail, Michael Equi, Chelsea Finn, Niccolò Fusai, Manuel Y. Gallicher, Dibya Ghosh, Lachy Groom, Karol Hausman, Brian Ichter, Szymon Jakubczak, Tim Jones, Liyiming Ke, Devin LeBlanc, Sergey Levine, Adrian Li-Bell, Mohith Mothukuri, Suraj Nair, Karl Pertsch, Allen Z. Ren, Lucy Xiaoyang Shi, Laura Smith, Jost Tobias Springenberg, Kyle Stachowicz, James Tanner, Quan Vuong, Homer Walke, Anna Walling, Haohuan Wang, Lili Yu, and Ury Zhilinsky. $\pi_{0.5}$: a vision-language-action model with open-world generalization, 2025. 3, 6
- [20] Yunfan Jiang, Agrim Gupta, Zichen Zhang, Guanzhi Wang, Yongqiang Dou, Yanjun Chen, Li Fei-Fei, Anima Anandkumar, Yuke Zhu, and Linxi Fan. Vima: General robot manipulation with multimodal prompts. *arXiv preprint arXiv:2210.03094*, 2(3):6, 2022. 1
- [21] Yunfan Jiang, Ruohan Zhang, Josiah Wong, Chen Wang, Yanjie Ze, Hang Yin, Cem Gokmen, Shuran Song, Jiajun Wu, and Li Fei-Fei. Behavior robot suite: Streamlining real-world whole-body manipulation for everyday household activities, 2025. 6
- [22] Moo Jin Kim, Karl Pertsch, Siddharth Karamcheti, Ted Xiao, Ashwin Balakrishna, Suraj Nair, Rafael Rafailov, Ethan Foster, Grace Lam, Pannag Sanketi, et al. Openvla: An open-source vision-language-action model. *arXiv preprint arXiv:2406.09246*, 2024. 1, 2
- [23] Chengshu Li, Fei Xia, Roberto Martín-Martín, Michael Lin-gelbach, Sanjana Srivastava, Bokui Shen, Kent Vainio, Cem

- Gokmen, Gokul Dharan, Tanish Jain, et al. igibson 2.0: Object-centric simulation for robot learning of everyday household tasks. *arXiv preprint arXiv:2108.03272*, 2021. 2
- [24] Chengshu Li, Ruohan Zhang, Josiah Wong, Cem Gokmen, Sanjana Srivastava, Roberto Martín-Martín, Chen Wang, Gabrael Levine, Wensi Ai, Benjamin Martinez, et al. Behavior-1k: A human-centered, embodied ai benchmark with 1,000 everyday activities and realistic simulation. *arXiv preprint arXiv:2403.09227*, 2024. 2
- [25] Qixiu Li, Yaobo Liang, Zeyu Wang, Lin Luo, Xi Chen, Mozheng Liao, Fangyun Wei, Yu Deng, Sicheng Xu, Yizhong Zhang, et al. Cogact: A foundational vision-language-action model for synergizing cognition and action in robotic manipulation. *arXiv preprint arXiv:2411.19650*, 2024. 2
- [26] Xiaoqi Li, Mingxu Zhang, Yiran Geng, Haoran Geng, Yuxing Long, Yan Shen, Renrui Zhang, Jiaming Liu, and Hao Dong. Manipllm: Embodied multimodal large language model for object-centric robotic manipulation. In *Proceedings of the IEEE/CVF Conference on Computer Vision and Pattern Recognition*, pages 18061–18070, 2024. 1, 2
- [27] Jiaming Liu, Hao Chen, Pengju An, Zhuoyang Liu, Renrui Zhang, Chenyang Gu, Xiaoqi Li, Ziyu Guo, Sixiang Chen, Mengzhen Liu, et al. Hybridvla: Collaborative diffusion and autoregression in a unified vision-language-action model. *arXiv preprint arXiv:2503.10631*, 2025. 3
- [28] Shilong Liu, Zhaoyang Zeng, Tianhe Ren, Feng Li, Hao Zhang, Jie Yang, Qing Jiang, Chunyuan Li, Jianwei Yang, Hang Su, et al. Grounding dino: Marrying dino with grounded pre-training for open-set object detection. In *European conference on computer vision*, pages 38–55, 2024. 2
- [29] Ajay Mandlekar, Danfei Xu, Josiah Wong, Soroush Nasiriany, Chen Wang, Rohun Kulkarni, Li Fei-Fei, Silvio Savarese, Yuke Zhu, and Roberto Martín-Martín. What matters in learning from offline human demonstrations for robot manipulation, 2021. 6
- [30] Soroush Nasiriany, Abhiram Maddukuri, Lance Zhang, Adeet Parikh, Aaron Lo, Abhishek Joshi, Ajay Mandlekar, and Yuke Zhu. Robocasa: Large-scale simulation of everyday tasks for generalist robots. *arXiv preprint arXiv:2406.02523*, 2024. 2, 5
- [31] Abby O'Neill, Abdul Rehman, Abhiram Maddukuri, Abhishek Gupta, Abhishek Padalkar, Abraham Lee, Acorn Poooley, Agrim Gupta, Ajay Mandlekar, Ajinkya Jain, et al. Open x-embodiment: Robotic learning datasets and rt-x models: Open x-embodiment collaboration 0. In *2024 IEEE International Conference on Robotics and Automation (ICRA)*, pages 6892–6903, 2024. 2
- [32] Alec Radford, Jong Wook Kim, Chris Hallacy, Aditya Ramesh, Gabriel Goh, Sandhini Agarwal, Girish Sastry, Amanda Askell, Pamela Mishkin, Jack Clark, et al. Learning transferable visual models from natural language supervision. In *International conference on machine learning*, pages 8748–8763, 2021. 2
- [33] Charan Ranganath and Maureen Ritchey. Two cortical systems for memory-guided behaviour. *Nature reviews neuroscience*, 13(10):713–726, 2012. 1
- [34] Scott Reed, Konrad Zolna, Emilio Parisotto, Sergio Gomez Colmenarejo, Alexander Novikov, Gabriel Barth-Maron, Mai Gimenez, Yury Sulsky, Jackie Kay, Jost Tobias Springenberg, et al. A generalist agent. *arXiv preprint arXiv:2205.06175*, 2022. 1
- [35] Hao Shi, Bin Xie, Yingfei Liu, Lin Sun, Fengrong Liu, Tiancai Wang, Erjin Zhou, Haoqiang Fan, Xiangyu Zhang, and Gao Huang. Memoryvla: Perceptual-cognitive memory in vision-language-action models for robotic manipulation. *arXiv preprint arXiv:2508.19236*, 2025. 3
- [36] Mohit Shridhar, Lucas Manuelli, and Dieter Fox. Cliport: What and where pathways for robotic manipulation. In *Conference on robot learning*, pages 894–906, 2022. 1
- [37] Sanjana Srivastava, Chengshu Li, Michael Lingelbach, Roberto Martín-Martín, Fei Xia, Kent Elliott Vainio, Zheng Lian, Cem Gokmen, Shyamal Buch, Karen Liu, et al. Behavior: Benchmark for everyday household activities in virtual, interactive, and ecological environments. In *Conference on robot learning*, pages 477–490, 2022. 2
- [38] Andrew Szot, Alexander Clegg, Eric Undersander, Erik Wijsmans, Yili Zhao, John Turner, Noah Maestre, Mustafa Mukadam, Devendra Singh Chaplot, Oleksandr Maksymets, et al. Habitat 2.0: Training home assistants to rearrange their habitat. *Advances in neural information processing systems*, 34:251–266, 2021. 2
- [39] Octo Model Team, Dibya Ghosh, Homer Walke, Karl Pertsch, Kevin Black, Oier Mees, Sudeep Dasari, Joey Hejna, Tobias Kreiman, Charles Xu, et al. Octo: An open-source generalist robot policy. *arXiv preprint arXiv:2405.12213*, 2024. 1
- [40] Jun Wang, Dongyan Guo, et al. Pointattn: You only need attention for point cloud completion. In *Proceedings of the AAAI Conference on Artificial Intelligence*, 2023. 4
- [41] Junjie Wen, Yichen Zhu, Jinming Li, Zhibin Tang, Chaomin Shen, and Feifei Feng. Dexvla: Vision-language model with plug-in diffusion expert for general robot control. *arXiv preprint arXiv:2502.05855*, 2025. 3
- [42] Jimmy Wu, Rika Antonova, Adam Kan, Marion Lepert, Andy Zeng, Shuran Song, Jeannette Bohg, Szymon Rusinkiewicz, and Thomas Funkhouser. Tidybot: Personalized robot assistance with large language models. *Autonomous Robots*, 47(8):1087–1102, 2023. 2
- [43] Jimmy Wu, William Chong, Robert Holmberg, Aaditya Prasad, Yihuai Gao, Oussama Khatib, Shuran Song, Szymon Rusinkiewicz, and Jeannette Bohg. Tidybot++: An open-source holonomic mobile manipulator for robot learning. *arXiv preprint arXiv:2412.10447*, 2024. 2, 6
- [44] Yanjie Ze, Gu Zhang, Kangning Zhang, Chenyuan Hu, Muhan Wang, and Huazhe Xu. 3d diffusion policy: Generalizable visuomotor policy learning via simple 3d representations, 2024. 2, 6, 3
- [45] Xiaohua Zhai, Basil Mustafa, Alexander Kolesnikov, and Lucas Beyer. Sigmoid loss for language image pre-training, 2023. 4
- [46] Pingrui Zhang, Xianqiang Gao, Yuhua Wu, Kehui Liu, Dong Wang, Zhigang Wang, Bin Zhao, Yan Ding, and Xuelong Li. Moma-kitchen: A 100k+ benchmark for affordance-

- grounded last-mile navigation in mobile manipulation. *arXiv preprint arXiv:2503.11081*, 2025. 2
- [47] Tony Z Zhao, Vikash Kumar, Sergey Levine, and Chelsea Finn. Learning fine-grained bimanual manipulation with low-cost hardware. *arXiv preprint arXiv:2304.13705*, 2023. 1
- [48] Brianna Zitkovich, Tianhe Yu, Sichun Xu, Peng Xu, Ted Xiao, Fei Xia, Jialin Wu, Paul Wohlhart, Stefan Welker, Ayaan Wahid, et al. Rt-2: Vision-language-action models transfer web knowledge to robotic control. In *Conference on Robot Learning*, pages 2165–2183, 2023. 1, 2

A. More implementation details of the real-world experiments

Our real-robot experiments were conducted using four commonly encountered household objects, as illustrated in Fig. 6. These objects were selected to cover diverse manipulation skills, including pulling, pushing, opening, and placing. The refrigerator measures **46 cm × 50 cm × 102 cm** (length–width–height) and contains both upper and lower doors with independent handles. The microwave oven is **43 cm × 30 cm × 26 cm**, with a side-opening door and rotary control knobs. A small cabinet with a pull-out drawer and a lower door measures **40 cm × 40 cm × 60 cm**. Finally, the stainless-steel sink setup, including the drying rack and basin, measures **100 cm × 50 cm × 89 cm**. These objects collectively provide a diverse set of physical interactions for evaluating long-horizon mobile manipulation performance.



Figure 6. The specific objects used in the real-world experiments.

In addition to the original TidyBot hardware configuration, we revised the placement of the bottom-facing camera. Specifically, we mounted an Intel RealSense D435i on the

robot base with an upward-looking orientation. This configuration enables the camera to reliably capture the motion of the manipulator end-effector throughout the execution of various tasks, providing clearer visual observations of fine-grained arm interactions during manipulation, as shown in Fig 8.

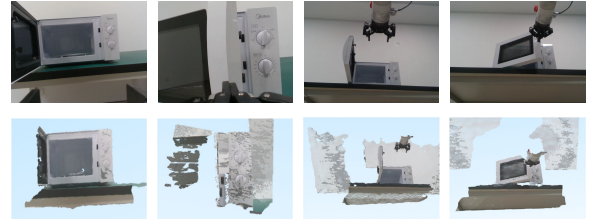


Figure 7. Representative examples of images and point cloud data collected from real robots.



Figure 8. Camera placement setup on the real-world robot experiments.

B. Training Hyperparameters

Table 4. Training hyperparameters used in our experiments.

Hyperparameter	Value
Optimizer	AdamW
Learning rate	1×10^{-4}
Batch size	128
Epochs	50
Warm-up steps	2,000
LR schedule	Cosine decay
Weight decay	0.01
Gradient clipping	1.0
Dropout rate	0.1
Diffusion steps	50
Noise prediction	ϵ -prediction
GPU setup	8×A100 (80GB)

To ensure stable and efficient training, we adopt the hyperparameter configuration summarized in Table 4. The

model is optimized using the AdamW optimizer with a learning rate of 1×10^{-4} , cosine learning-rate decay, and 2,000 warm-up steps. We train for 50 epochs with a batch size of 128, and apply a weight decay of 0.01 together with a dropout rate of 0.1 to prevent overfitting. Gradient clipping with a threshold of 1.0 is used to stabilize optimization. For the diffusion-based action decoder, we employ 50 denoising steps with standard ϵ -prediction. All experiments are conducted on a cluster of eight A100 (80GB) GPUs.

C. Additional Analysis of the MoMani Dataset

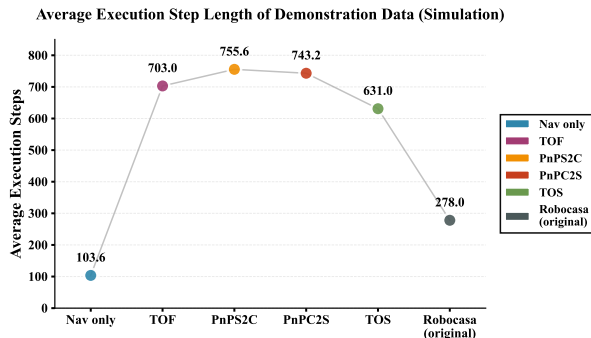


Figure 9. Average execution steps across different task datasets in simulation environment.

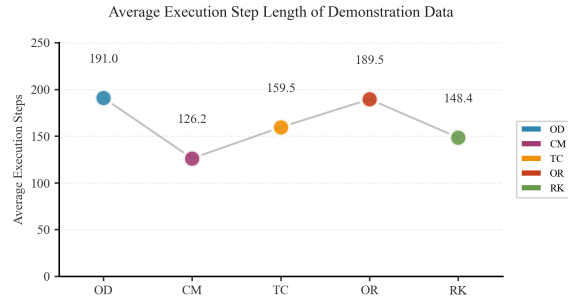


Figure 10. Average execution steps across different task datasets in real environment.

Figure 9 presents a quantitative comparison of the average execution steps across different task datasets in our simulation environment. Our proposed datasets (**TOF**, **PnPS2C**, **PnPC2S**, **TOS**) exhibit significantly longer trajectory horizons compared to the baseline Robocasa (original) dataset, with execution steps ranging from 630.99 to 755.56 steps versus 278.00 steps. This substantial increase in trajectory length reflects the enhanced complexity and long-horizon nature of our task formulations. Specifically, **PnPS2C** achieves the longest average trajectory with 755.56 steps, representing a $2.7 \times$ increase over the original dataset. The **Nav only** baseline (103.62 steps) serves as a lower bound, representing pure navigation without manipulation. These extended horizons necessitate more sophisticated planning and decision-making capabilities, making our datasets more challenging and more representative of real-world robotic manipulation scenarios.

In addition, Figure 14 reports the average execution steps collected in real-world experiments across four representative mobile manipulation tasks (OD, CM, TC, OR). The execution lengths vary notably between tasks, ranging from 126.2 to 191.0 steps, reflecting the differing physical complexities and interaction requirements of each scenario. Notably, tasks with more intricate object interactions—such as opening a drawer or refrigerator door—tend to require longer execution sequences. This real-world trend is consistent with our simulated dataset statistics, further validating the long-horizon characteristics and practical relevance of our proposed task designs.

D. Supplementary Illustrations of RoboCasa Tasks

Figure 15, Figure 16 and Figure 17 illustrate a series of navigation-and-manipulation tasks executed by our mobile manipulator in the RoboCasa environment. Each scenario showcases how the robot integrates visual perception, navigation planning, and fine-grained manipulation to reach target locations, interact with objects, and complete long-horizon tasks. The demonstrations highlight the diversity and complexity of RoboCasa tasks, ranging from simple spatial navigation to multi-step object interactions requiring precise coordination between the mobile base and the robotic arm.

E. Visualization of Voxelized 3D Feature Maps



Figure 11. The iterative process of constructing the voxelized point-cloud map.

Figure 11 illustrates the iterative construction process of our voxel-based feature map. Starting from raw point-cloud observations, the system progressively aggregates spatial information into a structured voxel representation, enabling stable feature extraction and efficient memory retrieval throughout the mapping procedure.

Figure 12 illustrates the spatial alignment between observed point clouds (top) and ground-truth environment reconstructions (bottom); the clouds faithfully preserve task-critical structures such as table edges and object contours.

Figure 13 illustrates that our point-cloud map memory mechanism successfully attends to task-relevant target objects during retrieval. However, we also observe an

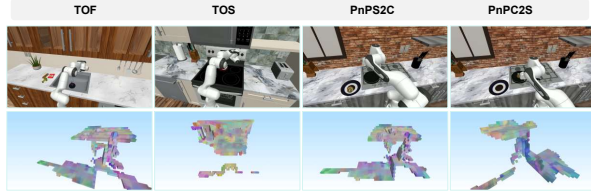


Figure 12. Observed-to-environment point-cloud alignment.

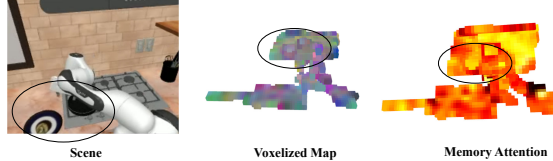


Figure 13. Visualization of point-cloud map memory retrieval.

unintended attention response toward parts of the robot’s own body—for example, the manipulator links and base frame—which occasionally appear as salient regions in the retrieved voxel features.

F. Additional Real-World Experiment: Rotating Microwave Knob

To further validate the generalization capability of our approach, we introduced an additional real-world task: **Rotating microwave Knob (RK)**. This task requires the robot to navigate to the microwave oven, precisely grasp the rotary control knob, and rotate it to adjust the cooking settings.

Table 5. Success rates on RK task in real-world experiments.

Method	RK
$\pi_{0.5}$	0.40
Diffusion	0.10
DP3	0.00
Ours	0.50

As reported in Table 5, our method attains a **50 %** success rate on the real-world RK task, outperforming both $\pi_{0.5}$ [19] (40 %) , Diffusion Policy [10] (10 %) and DP3 [44](0 %).

DP3 relies solely on single-view point clouds; as the camera moves with the base, its normalization collapses absolute depth, yielding near-identical states across frames. Coupled with the incomplete real point cloud, the model loses metric awareness and produces almost-garbled commands. Consequently, success rates on OD, CM, TC and RK are 0, except 0.1 on OR. In simulation, multi-view fused and complete depth is available, so performance remains high.

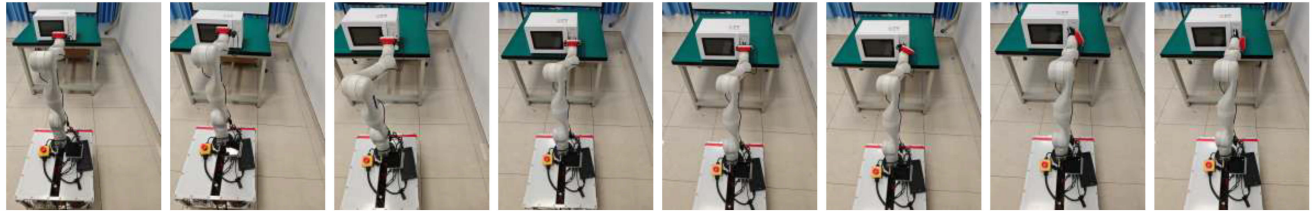


Figure 14. EchoVLA completes the task of rotating the microwave knob.

Pick the egg from the plate and place it in the pan then navigate to coffee machine.

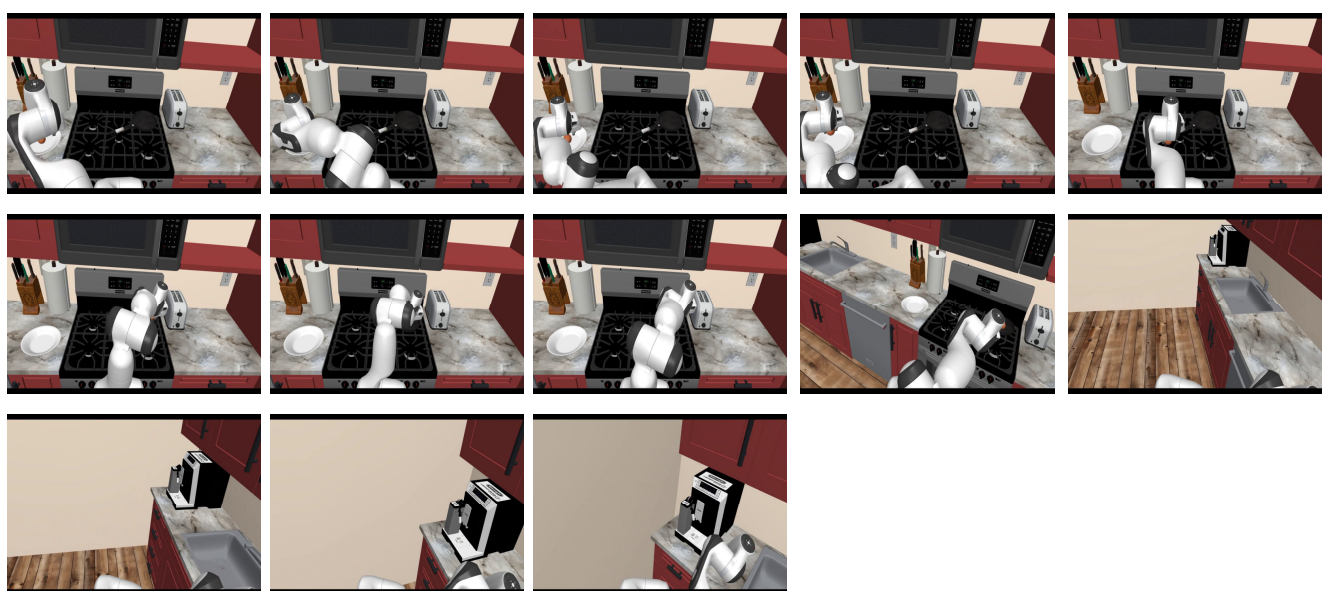
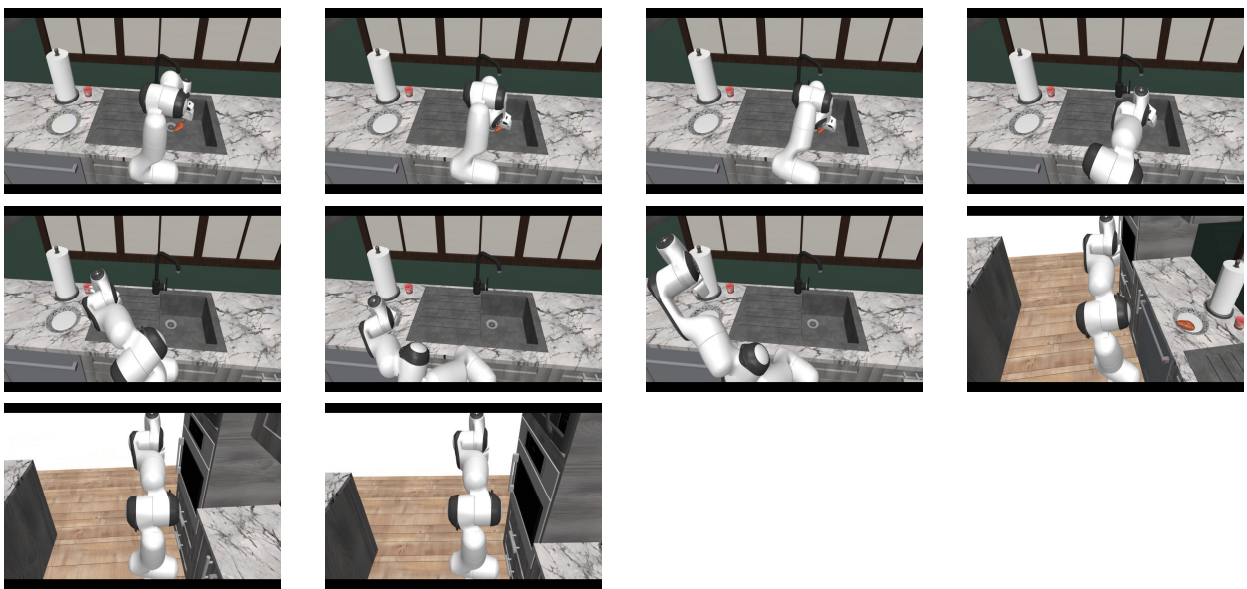


Figure 15. Example of a navigation-and-manipulation task in RoboCasa.

Pick the carrot from the sink and place it on the plate located on the counter then navigate to corner cabinet.



Turn on the sink faucet then navigate to cabinet near fridge.

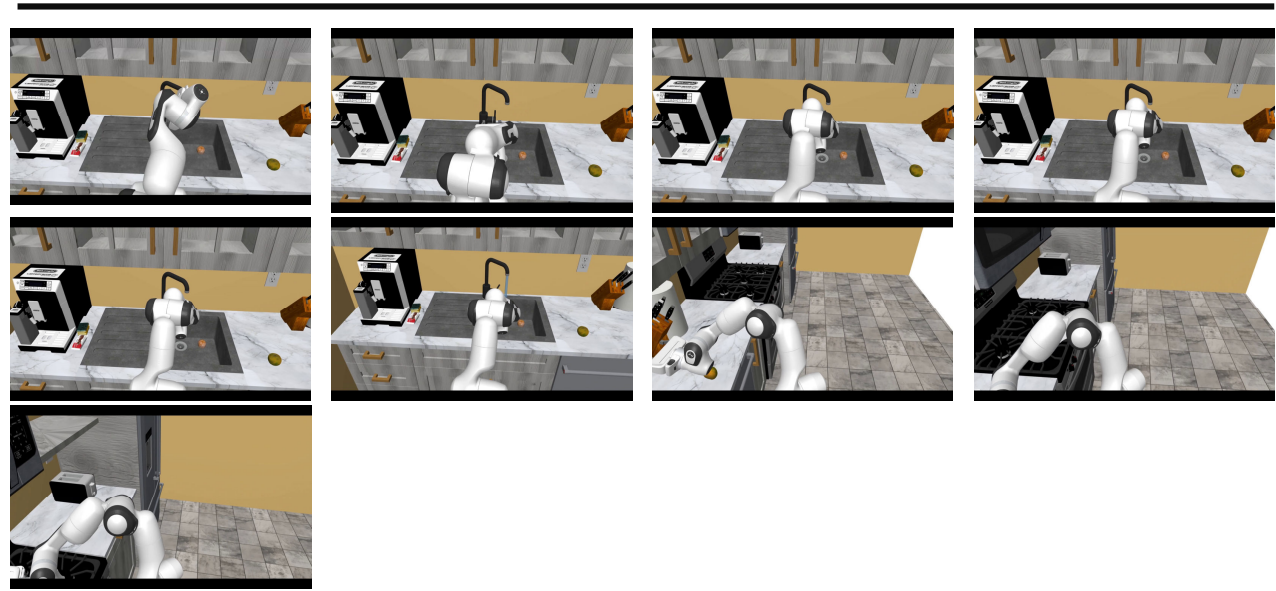
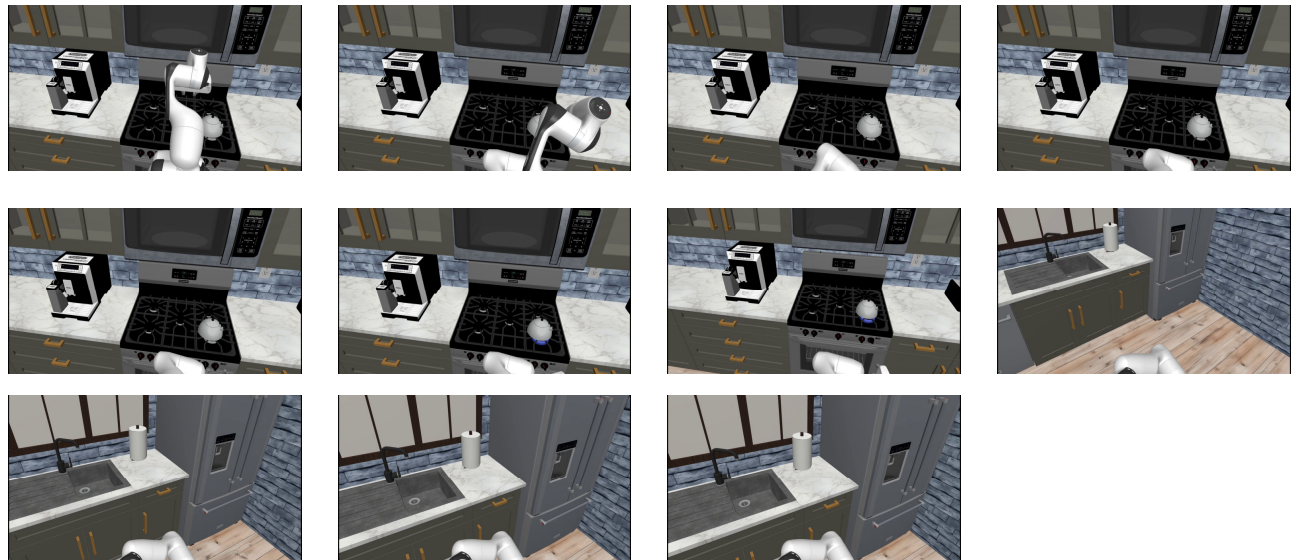


Figure 16. Example of a navigation-and-manipulation task in RoboCasa.

Turn on the sink faucet then navigate to cabinet near fridge.



Navigate to the cabinet and then pick the eggplant from the plate and place it in the pan



Figure 17. Example of a navigation-and-manipulation task in RoboCasa.